

Effects of Price Range Variation on Optimal Sizing and Energy Management Performance of a Hybrid Fuel Cell Vehicle

Alvaro Macias, *Student Member, IEEE*, Mohsen Kandidayeni, *Student Member, IEEE*, Loïc Boulon, *Senior Member, IEEE*, João P. Trovão, *Senior Member, IEEE*

Abstract— The usage of multi-objective cost functions (MOCFs) in sizing and energy management strategy (EMS) of fuel cell hybrid electric vehicles (FCHEVs) has expanded due to the participation of multiple technological and economic disciplines. To better understand the impact of price fluctuation on the component size and EMS of an FCHEV, this article proposed a sensitivity analysis methodology. First, a two-step optimization approach that considers hydrogen consumption, system degradation, and trip cost is used to minimize a MOCF of the Can-Am Spyder electric motorcycle simulator. Then, an effect analysis is carried out for the cost-optimal results under two driving profiles to understand the link between cost variation and system performance. These simulations indicate that each might result in different system sizes and EMS compromise. After that, an online optimization EMS based on sequential quadratic programming is used on a reduced-scale hardware-in-the-loop configuration to evaluate the simulation results with varied weights. Experimental results indicate that when an adequate size is used for each pair of weights, the EMS results in a 6 % decrease in the trip cost.

Index Terms— Electric vehicles, fuel cells, genetic algorithms, multi-objective programming, optimal control

NOMENCLATURES

DP	Dynamic programming
EE	Elementary effects
EMR	Energetic macroscopic representation
EMS	Energy management strategy
FC	Fuel cell
FCHEV	Fuel cell hybrid electric vehicle
GA	Genetic algorithm
HIL	Hardware-in-the-loop
MOCF	Multi-objective cost function
SA	Sensitivity analysis
SC	Supercapacitor
SQP	Sequential quadratic programming
WMTC	World motorcycle test cycle

This work was supported in part by the Fonds de Recherche du Québec Nature et Technologies (FRQNT) (283370 & 284914), Réseau Québécois sur l'Énergie Intelligente (3rd cycle and postdoctoral scholarships), Natural Sciences and Engineering Research Council of Canada (NSERC) (Grant RGPIN-2018-06527 and RGPIN-2017-05924) and Canada Research Chairs program (Grant 950-230863 and 950-230672).

Alvaro Macias and Loïc Boulon are with the Hydrogen Research Institute, Department of Electrical and Computer Engineering, *Université du Québec à Trois-Rivières*, QC G8Z4M3, Canada (email: alvaro.omar.macias.fernandez@uqtr.ca, loic.boulon@uqtr.ca).

I. INTRODUCTION

A fuel cell hybrid electric vehicle (FCHEV) is composed of a proton exchange membrane fuel cell (FC), as the principal power source, and a battery and/or supercapacitor (SC), as the energy storage system [1]. This hybrid structure can supply the dynamic power demand, absorb the regenerative braking energy, and handle cold start issues provided that proper component sizing and energy management strategy (EMS) are designed [2]. An appropriate component sizing declines the overall ownership cost of a FCHEV while maintaining the expected performance. In [3], it is shown that determining the optimal battery and SC capacity according to the recuperation potential and FC dynamics can lead to small-sized battery and more stable FC operation. The use of an EMS is also necessary since the involved power/energy sources have different energetic characteristics in this hybrid powertrain. This strategy is supposed to distribute the power flow between the sources with the aim of minimizing the hydrogen consumption and maximizing the lifetime of the components. The presence of several objectives (technical, economic, environmental, and socio-political) in the design of a proper sizing and EMS makes the definition of a suitable cost function vital. Hence, the use of a multi-objective cost function (MOCF), based on an economic and system dimensions point of view, has been practiced in [4, 5]. A MOCF attempts to reach a compromise among the defined goals using the given importance or weights to each of the objectives. In [6], an economic comparison of a multi-objective hierarchical EMS against single objective ones is presented. The results shows that an equivalent consumption minimization strategy will regulate the FC to work in the optimal efficiency region, while the MOCF controls the output current of the FC to achieve an optimal balance between the FC degradation and hydrogen consumption. In [7], an economic assessment of a convex multicriteria optimization approach is implemented in a FC

Mohsen Kandidayeni is with Department of Electrical Engineering and Computer Engineering, *Université de Sherbrooke*, Sherbrooke, QC, J1K 2R1, Canada, and also with the Hydrogen Research Institute, Department of Electrical and Computer Engineering, *Université du Québec à Trois-Rivières*, QC G8Z4M3, Canada (e-mail: Mohsen.Kandidayeni@USherbrooke.ca).

João P. F. Trovão is with the Department of Electrical Engineering and Computer Engineering, *Université de Sherbrooke*, Sherbrooke, QC, J1K 2R1, Canada, and also with Polytechnic of Coimbra (IPC-ISEC) and INESC Coimbra, Portugal (e-mail: Joao.Trovao@USherbrooke.ca).

hybrid bus. The resulted pareto plots show that a balance between the FC lifetime and hydrogen consumption is necessary to reach the maximum benefits of the hybrid powertrains. In [8], a multi-objective design exploration shows that the FC size has a considerable effect on the overall vehicle performance and system degradation. However, these weights are normally specified based on the prices of components which are variable owing to different policies and technological advancement [9]. In this regard, sensitivity analysis (SA) has been successfully utilized in other research areas to clarify such interactions. The SA approaches can be mainly divided into two groups of local and global [10]. Local SA techniques investigate the effect of small perturbations around one point while the global ones consider a wider variation range of the inputs and analyze their influence over the whole feature space [11]. The performed SA approaches in the area of FCHEVs have mainly focused on the one-at-a-time method to identify the parameters or strategies that lead to the best result. In [12], a convex programming problem is formulated to optimize the power distribution and sizing of a plug-in FC urban logistics vehicle. In order to define the battery and FC sizes which in turn minimize the energy and power sources cost, a one-at-a-time SA is done based on different driving cycles and hydrogen prices. However, the authors have mainly focused on the performance of the EMS without paying attention to the real influence of the component prices. In [13], a multi-objective optimal problem, considering the decay of an electrochemical surface area model, fuel consumption and battery degradation, is developed using different weight factors. The obtained results show that assigning different factors to the FC degradation can change its operating function from a load-following to a more constant profile, which dramatically affects its lifetime. However as underlined in the article, future changes in the cost or degradation rates may yield different results. In [14], a sizing approach is implemented for FC electrified heavy-duty trucks and tested under different cost scenarios by defining total cost of ownership. The obtained results suggest that a FC powertrain will be more attractive than a pure battery one in 10 years according to current projections for the cost of FC system, battery pack, fuel storage, hydrogen, and electricity. In [15], a SA is performed for different initial battery SOC and energy prices to assess the effect of a multi-scheme EMS for a driven passenger ship. Another example is given in [16], where the influence of the modeling parameters on the dynamical performance of PEMFC is investigated. This study shows that the most sensitive parameters can mislead the polarization curve estimation from the real behavior.

So far, several methods have been proposed for determining the most appropriate combination of component sizes based on the hydrogen consumption, FC degradation or MOCFs. However, these works do not ponder the effect of weight variations on the cost function. Therefore, this paper proposed a methodology to scrutinize the impact of component price variation on the sizing and energy management of a FCHEV. The Morris or elementary effects (EE) method is used in this work due to its low computational within the feasible parameter space; the performance of this screening technique has already

been validated in other engineering problems [17]. This global SA is suitable for the systemic analysis of FCHEVs, mainly due to its ability to cope with complex systems (multiple criteria) with a low computational complexity compared with variance-based methods. However, special attention needs to be paid to selecting the EMS and sizing method to avoid misleading conclusions. In fact, the performance of an EMS depends on the system size because this size will define the operating range and the possible combination of the system states [18]. Therefore, in this work, a two-step optimization method with a nested structure is utilized to reach the global optima and remove any influence on the EMS or system size results during the SA. The nested or bi-level method is one of the most used methods to solve this coupled optimization problem in recently published papers since it reaches a system-level optimal solution by making a tradeoff between the two problems [19, 20]. This work employs genetic algorithm (GA) and dynamic programming (DP) to reach near-optimal sizing and optimal power splitting, respectively, in a multi-objective system-level optimization. Several simulations and experiments are carried out to verify the outcomes of this study.

The rest of the paper is organized as follows. First, the followed methodology is discussed in Section II. Then, the obtained results are discussed in Section III. Finally, the conclusion is given in Section IV.

II. METHODOLOGY

In this work, the vehicle under study is the Can-Am Spyder electric motorcycle, which has an electric motor (permanent magnet synchronous: 28 kW, 96 V) directly linked to the rear wheel. It is utilized as an experimental test bench in e-TESC laboratory at the University of Sherbrooke [21]. In this manuscript, the performance of this electric motorcycle is evaluated for a FC-SC semi-active architecture. To do so, a simulation stage and an experimental stage validation are considered. In the simulation stage, an experimental based vehicle, FC and SC models are utilized to develop a coupled sizing and EMS problem and conduct a SA on the price variation of the power supply system. Consequently, in the experimental stage, a reduced-scale hardware-in-the-loop (HIL) set-up is utilized to evaluate with a real-time EMS the sizing achieved in the simulation stage. Hereinafter, the modeling procedure of each stage is briefly explained.

A. Studied vehicle - powertrain model and simulation

FCHEVs are multi-physical systems that can be conveniently represented by energy-flow modeling approaches, such as energetic macroscopic representation (EMR). EMR uses causal graphic descriptions to show how energy is converted and exchanged in multi-energy domain systems. It has basic coupling elements that correspond to the multi-energy components and control elements that allow inversed model-based control loops to be deduced. Different colors and blocks reflect the interactions in the subsystems differently in EMR's graphical elements. Energy source, accumulation, conversion, and distribution are the four key elements employed in EMR to emphasize the system's energetic properties. The formalism of

EMR was initially presented in [22] and used in several other papers for FCHEVs [23]. Fig. 1 presents the forces acting on the vehicle alongside its moving direction (Fig. 1a) and the utilized FC-SC semi-active powertrain configuration (Fig. 1b). The vehicle dynamics and forces, shown in Fig. 1a, are divided into the mechanical transmission, chassis and environment interaction, shown in Fig. 1b. This was calculated using Newton's laws, as:

$$\frac{dV_{EV}}{dt} = \frac{(F_{tr} - F_{env})}{m_{eq} \sin \theta} \quad (1)$$

$$F_{tr} = (G_{gb}/r) T_{em} \eta_{gb}^\beta \quad (2)$$

$$F_{env} = F_{roll} + F_{grade} + F_{air} \quad (3)$$

$$F_{roll} = mg \mu_{fr} \cos \theta \quad (4)$$

$$F_{air} = 0.5 \rho_{air} A_{aero} C_d V_{EV}^2 \quad (5)$$

$$F_{grade} = mg \sin \theta \quad (6)$$

$$\Omega_m = (G_{gb}/r) V_{EV} \quad (7)$$

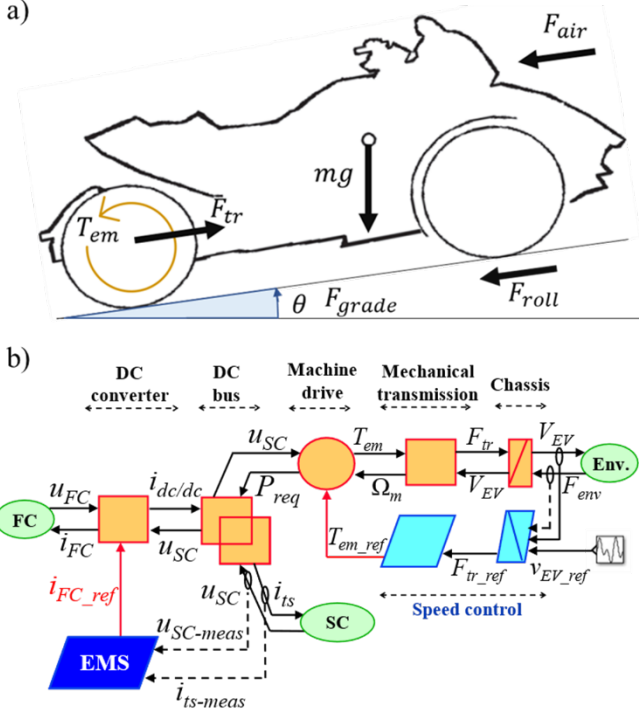


Fig. 1 The studied vehicle, a) Can-Am Spyder electric motorcycle, and b) powertrain configuration modeling using EMR.

where V_{EV} is the vehicle velocity, F_{tr} is the traction force, F_{env} is the vehicle traction force resistance, m is the vehicle mass, G_{gb} is the gearbox transmission ratio, r is the wheel radius, T_{em} is the electric machine torque, η_{gb} is the gearbox transmission efficiency, g is the gravitational acceleration, ρ_{air} is the air density, β is 1 in traction mode and -1 in braking mode, and Ω_m is the rotor rotation speed. It is worth mentioning that the vehicle mass includes an approximation of the mass of the chassis, passenger, powertrain and the energy sources. The mass of the energy/power sources are calculated based on the number of cells for the FC and SC arrangement [24].

The requested power (P_{req}), represented with a multi-physic conversion element, is calculated based on the torque and drive efficiency (η_m) that considers the inverter and motor efficiency by:

$$P_{req} = T_{em} \Omega_m \eta_m^\beta \quad (8)$$

The relationship of P_{req} , effective FC power ($P_{FC,bus}$), and SC power (P_{SC}) observed in the DC bus can be defined by:

$$P_{req} = P_{FC,bus} + P_{SC} \quad (9)$$

The FC stack performance is modeled by an electrochemical model proposed by Amphlett et al., [25] which was successfully implemented with experimental data in several papers [26]. In this work, the FCvelocity-9SSL from Ballard Power Systems has been chosen as the main power supply system due to the different available sizes, from 3.8 kW to 27.3 kW. The cell voltage (u_{FC}) of a proton exchange membrane type FC is approximated as (10-14):

$$u_{FC} = N_{FC} (E_{Nernst} + u_{act} + u_{ohmic} + u_{con}) \quad (10)$$

$$E_{Nernst} = 1.229 - 0.85 \times 10^{-3} (T_{FC} - 298.15) + 4.3085 \times 10^{-5} T_{FC} [\ln(p_{H_2}) + 0.5 \ln(p_{O_2})] \quad (11)$$

$$\begin{cases} u_{act} = \xi_1 + \xi_2 T_{FC} + \xi_3 T_{FC} \ln(CO_2) + \xi_4 T_{FC} \ln(i_{FC}) \\ C_{O_2}^* = \frac{P_{O_2}}{5.08 \times 10^6 \exp(-498/T_{FC})} \end{cases} \quad (12)$$

$$u_{ohmic} = -i_{FC} R_{internal} = -i_{FC} (\zeta_1 + \zeta_2 T_{FC} + \zeta_3 i_{FC}) \quad (13)$$

$$u_{con} = \alpha \ln(1 - i_{FC}/i_{FC,max}) \quad (14)$$

where u_{FC} is calculated with the number of cells (N_{FC}), the reversible voltage (E_{Nernst}), and the irreversible voltage losses composed of the activation loss (u_{act}), ohmic loss (u_{ohmic}), and concentration loss (u_{con}). The voltage components are in function of the operating current (i_{FC}), stack temperature (T_{FC}), hydrogen partial pressure (p_{H_2}), oxygen partial pressure (p_{O_2}), activation empirical coefficients (ξ_n), oxygen concentration ($C_{O_2}^*$), internal resistor ($R_{internal}$) defined by the three parametric coefficients ζ_n ($n = 1 \dots 3$), a semi-empirical parameter related to the diffusion mechanism (α), and the maximum current ($i_{FC,max}$). More information about each of these parameters can be found in [20].

The effective power of the FC system in the DC bus is calculated by using the efficiency ratio (η_{DC-DC}) of the DC-DC converter and the consumed power by the auxiliaries; composed of the fan cooling system (P_{fan}) and the power of the compressor (P_{comp}), as follow:

$$P_{FC,bus} = (i_{FC} \cdot u_{FC}) \eta_{DC-DC} - P_{comp} - P_{fan} \quad (21)$$

Moreover, the hydrogen flow (W_{H_2}) is approximated based on a linear function of the requested FC current as follow:

$$W_{H_2} = 0.00696 i_{FC} N_{FC} \quad (18)$$

A classical RC model represents the SC energy block due to the ease of calculation and a good approximation of the system behavior [27]. The electrical behavior is calculated as:

$$u_{SC}(t) = u_c(0) + \frac{1}{C_{SC}} \int i_{SC} dt - i_{SC} R_{SC} \quad (19)$$

where the SC voltage ($u_{SC}(t)$) is a function of the initial open-circuit voltage ($u_c(0)$) and the current across the SC (i_{SC}). The values of equivalent capacitance (C_{SC}), and the equivalent resistor of the SC (R_{SC}) are reported in the Maxwell Technologies manufacturer datasheet. The remaining energy in the SC is estimated by the formula of Coulomb counting, where $SOC_{SC}(0)$ represents the initial level of charge, and Q_{max} is the maximum capacity [28].

$$SOC_{SC}(t) = SOC_{SC}(0) + \int \frac{i_{SC} dt}{Q_{max}} \quad (20)$$

B. Hardware-in-the-loop set-up

Compared to real-vehicle tests, HIL is an attested, cost-effective procedure for designing an EMS. Moreover, the repeatability of the same case studies is a real plus to HIL simulation against on-road test facilities [29]. The developed HIL set-up for evaluating the performance of the vehicle model using different online EMSs is presented in Fig. 2. This HIL test bench is exactly based on the explained vehicle model in Fig. 1, in which the FC model has been replaced with an open cathode proton exchange membrane FC H-500 from Horizon company.

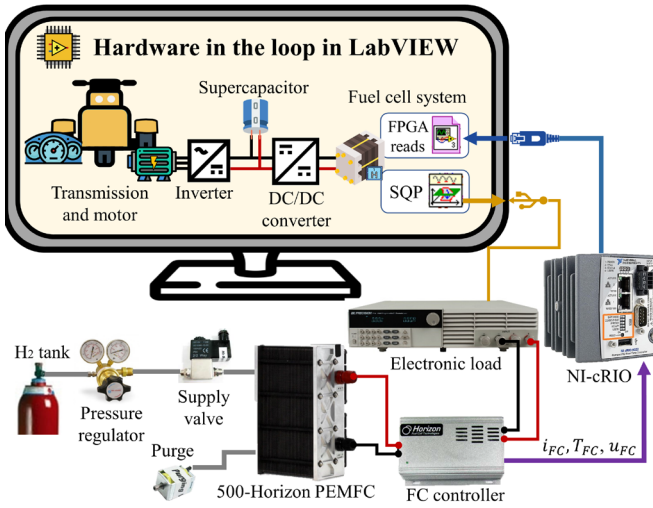


Fig. 2 The developed HIL set-up for evaluating the vehicle performance.

The FC controller handles the affixed axial fan, hydrogen valve, and purge valve. The axial fan has a dual role of cooling down the stack temperature and providing the required oxygen for the reactions. The information between the CompactRIO and the PC is transferred by an Ethernet connection with a rate of 10 Hz. A DC Electronic Load (8514 BK Precision) is employed to demand the imposed load profile by the DC-DC converter from the FC stack.

C. Nested optimization method

The utilized optimization method has two nested loops. The first (outer) one uses GA to minimize the cost function by finding the right decision variables (size of powertrain components). The second (inner) employs DP to optimally distribute the power using the obtained sizes in the first loop.

GA is appropriate for optimization problems in which the cost function is nonlinear, discontinuous, nondifferentiable, or stochastic. Two important components of the GA are the decision variables and the cost function. The decision variables in the sizing problem of this work are limited to the number of cells forming the FC stack (N_{FC}), the capacitance of a single SC ($C_{SC,u}$), the number of SC connected in series ($N_{SC,s}$), and the number of SC series banks in parallel ($N_{SC,p}$). GA is expected to minimize the following MOCF by tuning the mentioned variables. The trip cost is in terms of USD and comprises the costs of fuel consumption and wear of the system. The FC portion is linked to the system degradation, which is considered as the percentage of reduction in the maximum power. A dynamic operation of the FC significantly affects its durability and performance by corroding its key components resulting in the degradation of platinum catalyst and increment of the mass transfer resistance [30]. The SC and DC-DC converter, however, are predicted to last for thousands of cycles under typical circumstances [31]. Hence, their costs are only correlated with the trip time to increase their impact on the optimization process.

$$\begin{aligned} \$Trip = & \$FC_{sys} \Delta_{FC} + \$H_2 \int W_{H_2} dt + \$SC \Delta_{trip} + \\ & \$DC_{conv} \Delta_{trip} \end{aligned} \quad (22)$$

where the trip cost ($\$Trip$) in USD is composed of the FC system degradation cost ($\$FC_{sys}$: FC system cost based on its maximum power, Δ_{FC} : FC power degradation), the hydrogen consumption cost ($\$H_2$: Hydrogen cost per kilogram, W_{H_2} : hydrogen flow in SLPM), SC operational cost ($\$SC$: SC cost based on the total capacity, Δ_{trip} : trip time), and DC-DC converter operational cost ($\$DC_{conv}$: DC-DC converter cost based on the FC maximum power). However, the direct measurement of some internal parameters to monitor the FC/SC degradation are very challenging in real-time applications. In this respect, an indirect estimation can be done with mathematical models approaches, mainly group in white-box, black-box, and grey-box methods [32]. In [33], it is explained that the FC degradation is normally estimated with a semi-empirical model that consider the voltage drop at the stack level and extrapolate it by the number of cells. A similar approach has been done in [8, 34], where a stochastic dynamic programming strategy quantifies the FC degradation rates in terms of volts to compare different sizes in a common ground. In order to have a direct comparison of FC degradation between different FC sizes, it has been opted to translate the percentage of FC degradation to its equivalent in power decay caused by degradation. In the presented work, the power decay (Δ_{FC}) is calculated as a sum of effect from the different load conditions based on the empirical coefficients of a percentage FC performance degradation [35, 36].

$$\Delta_{FC} = P_{FC,max} (k_1 t_1 + k_2 n_1 + k_3 n_2 + k_4 t_2 + k_5 t_3) \quad (23)$$

where $P_{FC,max}$ is the FC maximum power, k_1 (0.00126 %/h) is the degradation rate due to low-power operation (less than 5 % of FC maximum power), k_2 (0.00196 %/cycle) is the degradation rate of one on/off cycle,

k_3 ($5.93 \times 10^{-5} \%$ /cycle) is the degradation rate of transient load changes, k_4 is the degradation rate of high-power operation (more than 90 % of FC maximum power), and k_5 (0.002 %/h) is the natural performance decay rate. t_1 , t_2 , and t_3 are the operation time in low-power, high-power, and FC on conditions respectively while n_1 is the number of on/off cycles and n_2 is the number of transient load changes [33]. According to the US Department of Energy (DOE), FC end of life (EOL) is defined as a 10 % decline in the maximum power with an operational objective of 5000 hours [37]. However, the SC and power components are expected to last around thousands of cycles in normal conditions [31]. Therefore, their cost is linked to the above-defined trip time (Δt_{trip}) to increase their importance in the optimization process, which is the total time divided by the operational objective of 5000 hours. It should be noted that the price of the system cost components ($\$FC_{sys}$, $\$H_2$, $\$SC$, and $\$DC_{conv}$) is variable in the market.

The decision variables used for the optimization problem are defined as discrete values based on the commercial capacitance of Maxwell SC and the size of the Ballard FC. This work focuses on the FCvelocity-9SSL model in which the number of cells defines the maximum power N_{FC} . Table I shows the search space formed by the decision variable ranges. Regarding the GA, the available function in the Optimization Tool of MATLAB is utilized while considering the following setting: Population size 200, maximum generations 200, Elite count 10, Selection function: “selectionstochunif”, and Crossover fraction: 0.8.

TABLE I DISCRETE DECISION VARIABLES RANGE

Variable	Search space
N_{FC}	[55,71,75,80,90,110,115,135]
$C_{SC,u}$	[100,150,310,325,350,360,450,650,1200,1500,2000,3000,340]
$N_{SC,s}$	$\in Z \geq 1, \leq 60$
$N_{SC,p}$	$\in Z \geq 1, \leq 60$

The FCHEV model is a nonlinear state-space model which DP can solve as one of the most well-known optimal control methods for nonlinear, time-variant, constrained, discrete-time models. DP solves an optimization problem by breaking it down into simpler subproblems assuming that the optimal solution to the overall problem is achieved by calculating the optimal solution to its subproblems. In this work, a DP function introduced in [38, 39] is used, which has been proposed for optimal energy management of FCHEVs. This method works based on calculating the boundary range of the state variable, dividing the state variables space into four operational modes, determining the minimum cost of each grid point forward, and calculating the minimum optimal control decision sequence backward. By doing so, this method shows less computational time and better calculation accuracy. The state-space for the current variable in this work is divided with a grid size of 0.5 A and the SOC space is divided with a grid size of 0.05 %. Using this DP function, the unified state-space equation of the vehicle under study can be described by the following four states:

$$\begin{cases} SOC_{SC}(k+1) = SOC_{SC}(k) + \int \frac{i_{SC}(k) dk}{Q_{max}} \\ u_{SC}(k+1) = u_c(k) + \frac{1}{C_{SC}} \int i_{SC}(k) dk - i_{SC}(k) R_{SC} \\ P_{FC,s}(k+1) = u_{FC}(k) * i_{FC}(k) \\ M(k+1) = \psi(P_{FC,s}, i_{FC}, k) \end{cases} \quad (24)$$

where SOC_{SC} is the SC SOC, u_{SC} is the SC voltage, $P_{FC,s}$ is the FC power, and M is the operational work mode. The considered control variable is the FC current (i_{FC}) whose optimal trajectory is given by DP. It should be noted DP uses the defined cost function in (22) to solve this optimization problem. The defined work mode is a function of the control variable (FC current) and the FC power which is a state variable. Definition of the work mode results in the reduction of the computational burden by avoiding the extra calculation for the infeasible areas.

To ensure that the system operates in the desired conditions, some limitations need to be imposed on the state and control variables as:

$$\begin{cases} 50 \% \leq SOC_{SC} \leq 90 \% \\ 0A \leq i_{FC} \leq 300 A \\ -300 A \leq i_{SC} \leq 300 A \\ 80 V \leq u_{DC} \leq 120 V \\ -0.1 P_{FC,max} \leq \Delta P_{FC} \leq 0.1 P_{FC,max} \end{cases} \quad (25)$$

where SOC_{SC} range is selected based on the requirements of the installed electric motor on Spyder vehicle. Since SC SOC has a direct relationship with voltage, the minimum and maximum ranges have been defined by considering the input voltage range of the motor driver (80 V – 120 V) in the optimization process. The current limits are based on the manufacturer’s manual, the u_{DC} range is defined based on the motor driver operating voltage, and the ΔP_{FC} is the slew rate of the FC power given by:

$$\Delta P_{FC} = P_{FC}(k) - P_{FC}(k-1) \quad (26)$$

D. Sensitivity Analysis

SA studies how uncertainty in the input parameters of a model affects the output response, identify the parameters with a significant influence on the model output and their interaction level. The literature review shows that the EE method is a good representation of the total sensitivity index because it evaluates the influence and interaction effect of each independent input parameter [11]. The calculation of the EE starts by discretizing the input variable space Ω of the model $y = f(\mathbf{X})$ in p levels. \mathbf{X} represents the independent input parameters $X_i, i = 1, \dots, k$ with k dimensions. The EE of the i th parameter is defined as:

$$E_i = \frac{[f(X_1, X_2, \dots, X_i + \Delta, \dots, X_k) - f(X_1, X_2, \dots, X_k)]}{\Delta} \quad (27)$$

where $\Delta = p/[2(p-1)]$ is the sampling step between $\{0,1\}$ that assures an equal probability of the p samples. It is recommended to set an even value for p . The number of points in the input space to evaluate is $(k+1)$ because a based value \mathbf{X}^* is included, which is defined as the initial coordinate to generate all the trajectory points. Therefore, the EE is calculated by two consecutive sets of input variables whose relative

distance in the coordinate X_i is Δ .

From the calculated EE, two sensitivity indices can be obtained:

$$\mu_i^* = \frac{1}{r} \sum_{j=1}^r |E_i^j| \quad (28)$$

where r denotes the number of trajectories with a recommended value between $\{4, 10\}$, μ_i^* is the mean of the absolute values that represents the influence of the variable on the output.

In order to improve the scanning of the input domain, the trajectories need to be spread in all the variable space Ω . In this sense, the design of trajectories can be done randomly, as follow:

$$B^* = (J_{k+1,1}X^* + (\Delta/2)[(2B - J_{k+1,k})D^* + J_{k+1,k}])P^* \quad (29)$$

where X^* is the base vector randomly selected, B is a lower triangular matrix of ones whose dimension is $(k+1) \times k$, $J_{k+1,k}$ is a $(k+1) \times k$ matrix of 1's, D^* is a k -dimensional diagonal matrix in which each element is either +1 or -1 with equal probability, P^* is a k -by- k random permutation matrix of zeros in which each row contains one element equal to 1, and no two columns have 1's in the same position. P^* gives the order in which factors are moved and P^* sets whether the factors will increase or decrease their value along the trajectory. Moreover, the scanning can be improved by maximizing the distance between the trajectories, which is calculated in this way:

$$d_{ml} = \sum_{i=1}^{k+1} \sum_{j=1}^{k+1} \sqrt{\sum_{z=1}^k [X_z^{(i)}(m) - X_z^{(j)}(l)]^2} \quad (30)$$

where d_{ml} is the sum of the geometrical distance between all the pairs of points of two different trajectories m and l .

III. RESULTS AND DISCUSSION

In this section, several scenarios through two phases of simulation and experiments are considered to examine the performance of the presented Can-Am Spyder electric vehicle. In the simulation phase, the introduced MOCF is used to determine the right dimension of the powertrain components with the help of the two-step nested optimization. Since each element of the MOCF is influenced by a range of prices, a SA using the explained EE method is performed. Lastly, in the experiment phase, the HIL set-up is utilized to carry out an experimental test with the aim of examining the influence of a component price on a MOCF with an online EMS

A. Numerical simulation

In the numerical simulation stage, the introduced MOCF is first compared with two single-objective ones to realize their operational differences. Subsequently, the SA is performed. As mentioned earlier, the price of hydrogen, FC, and energy storage are the factors that can affect the system dimensions and operation strategy. In addition, these parameters vary depending on the retail, acquisition volume, and technology readiness level. Therefore, different existing prices in the literature are collected, as reported in Table II, to investigate the influence of the price range variation over the component sizing

process [9, 40].

TABLE II COST RANGE OF THE POWERTRAIN COMPONENTS

Variable	Range
$\$FC_{sys}$	40 $\$/kW$ to 210 $\$/kW$
$\$H_2$	2 $\$/kg$ to 15 $\$/kg$
$\$SC$	15 $\$/Wh$ to 30 $\$/Wh$
$\$DC_{con}$	50 $\$/kW$ to 150 $\$/kW$

To perform the numerical simulation, the standard World Motorcycle Test Cycle (WMTC) and an on-road driving test are utilized, as shown in Fig. 3

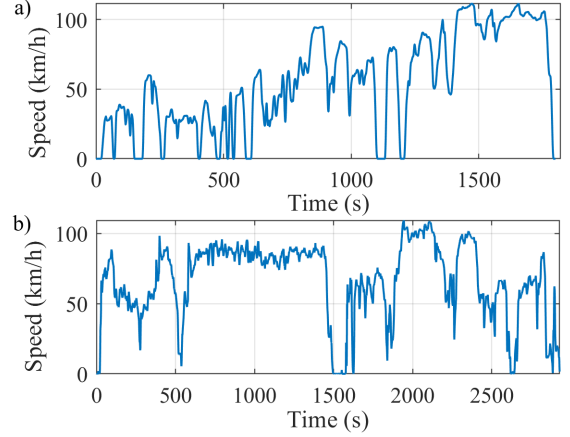


Fig. 3 Utilized driving profiles: (a) WMTC cycle, (b) on-road test.

WMTC represents daily motorcycle driving cycles in Europe, Japan, and the USA [41]. The real on-road driving test is about 49 minutes, reaching a top speed of 110 km/h. The vehicle operates mainly in the high-speed region in this driving profile. The average calculation time of the DP optimization step is 247 s for the WMTC profile, and for the on-road driving cycle is 342 s.

1) Cost function comparison

The utilized MOCF (22) in this study has four elements: FC degradation (23), hydrogen consumption (18), the operational cost of SC, and the operational cost of the DC-DC converter that are related to the (Δ_{trip}) trip time. The MOCF tries to reach a compromise among the objectives using a weighted sum approach [20]. Therefore, the price of each element defines the importance of each objective in terms of USD. In the first attempt, the MOCF is compared with two single-objective ones (hydrogen minimization: $H_{2,min} = \int W_{H_2} dt$ and FC degradation minimization: $FC_{deg,min} = \int \Delta_{FC} dt$), which represent the optimal limits of hydrogen and FC degradation minimization. In this regard, the extreme component prices, minimum and maximum from Table II, are considered for the MOCF. The maximum prices correspond to the actual component cost, and the minimum prices represent the objective values in the mid-term. In this way, the influence of the minimum and maximum prices over the size of the components will be appreciated. Regarding the single-objective cost functions, the inclusion of prices does not affect their performance as they pursue only one objective. Fig. 4 shows the optimization surfaces and pareto frontiers formed by different cost functions under WMTC driving cycle. This figure

represents trip cost (22) as the MOCF, and two single-objective: hydrogen consumption (18), and FC degradation (23). Fig. 4a shows the optimization surfaces of the MOCF with the extreme component prices, highest in orange at the top and lowest in blue at the bottom. The single points in each plot signify the GA population evaluated during the two-step optimization. Moreover, the surfaces show the pareto frontier with a continuous line, and the markers locate the best result coordinate in each case. The orange circle marker shows the minimum possible answer using the MOCF with the highest prices of the elements. The blue square marker presents the minimum result for the case of MOCF with the lowest prices for the elements. The single-objective functions were evaluated with the lowest component price and represented with a yellow hexagram marker for the best result obtained by the FC degradation minimization cost function, and the green diamond marker indicates the minimum result achieved by the hydrogen minimization cost function. From the next two subplots, Fig. 4b and Fig. 4c, it can be observed that although both MOCFs have different component prices, their pareto frontier converges to a pareto optimal point in the same optimal system size.

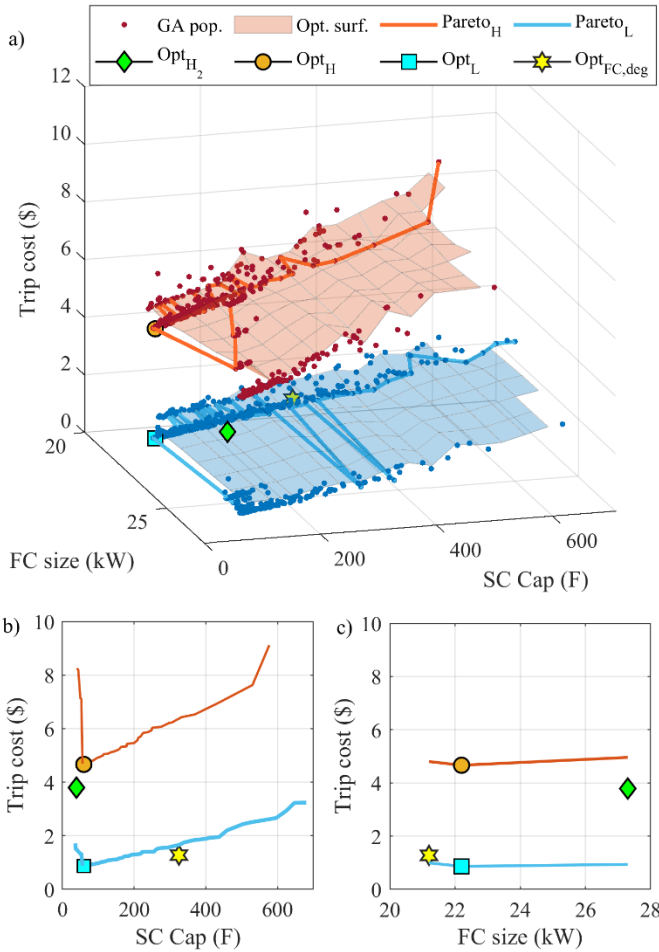


Fig. 4 Electric Spyder performance under WMTC driving cycle through two-step optimization method, a) multi-objective, b) Pareto frontier based on SC size and c) Pareto frontier based on FC size

This result shows that further analysis is required to comprehend the effect and interaction of price variation on the

sizing and operational cost. Therefore, a more detail analysis of the MOCF is presented next in Fig. 5 where special attention is paid on the hydrogen consumption and FC degradation component.

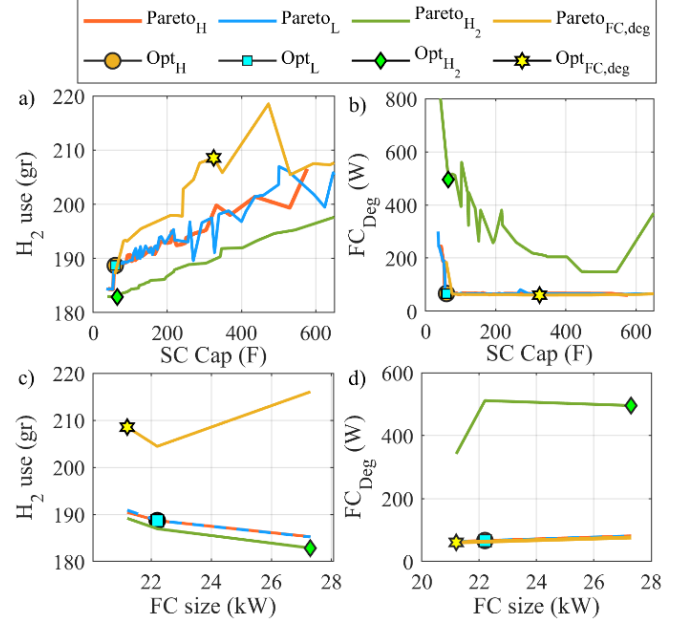


Fig. 5 Single-objective perspective of MOCF under WMTC driving cycle, a) hydrogen use vs SC size, b) FC deg. vs SC size, c) hydrogen use vs FC size and, d) FC deg vs FC size

The performance of the cost functions in terms of hydrogen consumption based on the SC and FC size are shown in Fig. 5a and Fig. 5c in terms of FC degradation and in terms of FC degradation in Fig. 5b and Fig. 5d. At first glance it is observed that the presented case is a nontrivial multi-objective optimization problem, where no single solution exists that simultaneously optimizes each single objective. This means that the components of the MOCF are in conflict, and none of them can be improved in value without declining some of the other objective values. From these plots, it can be observed that the single objective cost functions converge to the optimal solutions in their corresponded spaces while giving low-performance results in the other aspects. However, the optimal solutions obtained by the MOCF are near to the minimum results in both cases. To better interpret the performance of the explained cost functions in Fig. 4 and Fig. 5, the optimal results of each cost function are summarized in Table III. In addition, three MOCF with different components cost are included to highlight the influence of different set of weight in the cost function calculation. The extreme MOCF presents an increment of 3 % in terms of hydrogen consumption and 8% in terms of FC degradation, compared to the optimal results obtained by $H_{2,min}$ and $FC_{deg,min}$ cost functions, respectively. In addition, to reach a balance between both objectives, Table III shows that hydrogen minimization strategy will opt to use the highest FC size since the maximum efficiency power point will be higher, contrary to the FC degradation minimization that selects a smaller size to reduce the power decay caused by degradation. It should be noted that the FC degradation function has the biggest SC size because the bigger the filter the less the

degradation in the FC. At this point the obtained sizes and prices for the two price scenarios of MOCFs are similar. These results could mislead to conclude that the prices don't affect the system size, for this reason three weight sets with a minimum cost in one of the components is included in the Table III. When one of the components has a low cost, the system tends to operate as a single cost function, e.g., the MOCF with a low FC price has similar fuel performance as the $H_{2,min}$ function, which represents the optimal consumption. The MOCF is able to reach a balance although the weights are in the high or low extremes.

TABLE III COST FUNCTIONS COMPARISON UNDER WMTC DRIVING CYCLE

Cost function	H2 cons.	FC deg.	FC size	SC size (S-series and P-Parallel)
$H_{2,min}$	182.85 gr	496.8 W (0.0182 %)	27.3 kW	65.38 F (52S1P)
$FC_{deg,min}$	208.54 gr	61.5 W (0.0029 %)	21.2 kW	325 F (59S59P)
MOCF (lowest prices)	188.69 gr	66.6 W (0.003 %)	22.2 kW	59.6 F (49S9P)
MOCF (highest prices)	188.68 gr	66.6 W (0.003 %)	22.2 kW	59.6 F (49S9P)
MOCF (H2 cheap)	191.40 gr	63.6 W (0.003 %)	21.2 kW	122.7 F (48S19P)
MOCF (FC cheap)	185.16 gr	81.9 W (0.003 %)	27.3 kW	65 F (50S10P)
MOCF (SC cheap)	190.93 gr	63.6 W (0.003 %)	21.2 kW	103.3 F (16S48P)

From a wider perspective, a deeper analysis on the ratio of the FC and hydrogen price shows that the highest and lowest prices have similar weighting ratio. Under the low-cost conditions, the ratio of the hydrogen cost (2 \$/kg) to FC cost (40 \$/kW) is 1:20, while in the high-price conditions, the ratio of hydrogen cost (15 \$/kg) to FC cost (210 \$/kW) is 1:14. In case of the lowest prices scenario, the hydrogen cost is \$0.377 and the FC degradation cost is \$0.266, and in case of the highest cost scenario, the prices are \$2.83 and \$1.39, respectively. Based on the obtained trip cost, the ratio of the hydrogen to the FC degradation is 1.4:1 for the lowest price and 2:1 for the highest price. Under the tested driving cycle, it can be observed that although the FC has a higher ratio than the hydrogen, the hydrogen has a more considerable impact on the trip cost. Moreover, this analysis presents a very interesting perspective regarding the impact on the technology development and maturity where both technologies could reach similar trip cost influence at one instant.

Regarding the on-road driving cycle, sizing outcomes of two single-objective and three price sets (highest price, H2 cheap, and FC cheap) are analyzed and summarized in Table IV. The single objective functions set the baseline reference of the FC degradation and hydrogen consumption. The highest price shows the optimal dimension of the components for the highest reported prices in Table II. H2 cheap represents the optimal sizes using the highest prices for H_2 , SC , and DC_{con} , and the lowest price for FC_{sys} . FC cheap illustrates the optimal dimensions for the highest prices of FC_{sys} , SC , and DC_{con} , and the lowest price of H_2 . In fact, H2 cheap, and FC cheap cases simulate the situation in which one technology becomes cheaper faster than the others. From Table IV, when merely one weight is in the lowest extreme, the power distribution tends to

exploit its corresponding resource more (consume more hydrogen or degrade more the FC). These outcomes show that a SA is required to check each component's price change effect on the sizing and operating cost of the whole system. Since the technology evolution might not be at the same rate for all the components, they will take different values.

TABLE IV MULTI-OBJECTIVE COST FUNCTIONS COMPARISON UNDER ON-ROAD DRIVING CYCLE

MOCF	H2 cons.	FC deg.	FC size	SC size (S-series and P-Parallel)
$H_{2,min}$	337.38 gr	513.2 W (0.0188 %)	27.3 kW	75.5 F (45S1P)
$FC_{deg,min}$	398.16 gr	62.28 W (0.0036 %)	17.3 kW	364 F (50S28P)
MOCF (highest prices)	348.69 gr	76.3 W (0.0036 %)	21.2 kW	85.8 F (53S14P)
MOCF (highest prices)	347.25 gr	76.3 W (0.0036 %)	21.2 kW	88 F (48S13P)
MOCF (H2 cheap)	347.56 gr	76.3 W (0.0036 %)	21.2 kW	94.8 F (48S14P)
MOCF (FC cheap)	343.71 gr	124.3 W (0.0056 %)	22.2 kW	63.5 F (46S9P)
MOCF (SC cheap)	347.56 gr	76.3 W (0.0036 %)	21.2 kW	94.7 F (48S14P)

2) Sensitivity analysis

To clarify the effect of the price variation on the component sizing, the results of the EEs SA under WMTC and road-test driving cycles are discussed in this section. Fig. 6 presents the rank of each parameter in the center of the sub-square. The rank is defined using the mean of the absolute EEs values of the component prices. In this regard, the system performance in terms of hydrogen consumption (W_{H_2}), FC system degradation (Δ_{FC}), FC size ($P_{FC,max}$), SC size (C_{SC}), System mass ($m_{pow,sys}$), and total trip cost ($\$Trip$) is considered. From Fig. 6, the hydrogen and FC prices are the most influential parameters that almost overwhelm all other factors in both cases. In other words, a slight variation of these two parameters will have a considerable effect on the outputs. From the presented results in Fig. 6a, hydrogen is the most important parameter, and FC is the second most important one in the case of fuel efficiency for the WMTC driving cycle. This follows the results presented in Table III, where a low price of hydrogen generates an increment of 5 % in the fuel consumption. Moreover, the EE shows that the hydrogen price has a strong influence at defining the sizes of FC and SC. This point is also well represented in Table III, where it is shown that a low price in the FC will push the algorithm to choose the biggest FC size. Fig. 6b represents the obtained results regarding the SA under the road-test driving cycle. From this figure, the influence of the FC system cost increased compared to the WMTC driving cycle. The long-time operation reduces the percentage of fuel difference between the extreme cost function shown in Table IV, this means there is a change of importance due to the high speed and duration of the profile. However, it is observed that in both cases the hydrogen cost is the most influential parameter in term of trip cost.

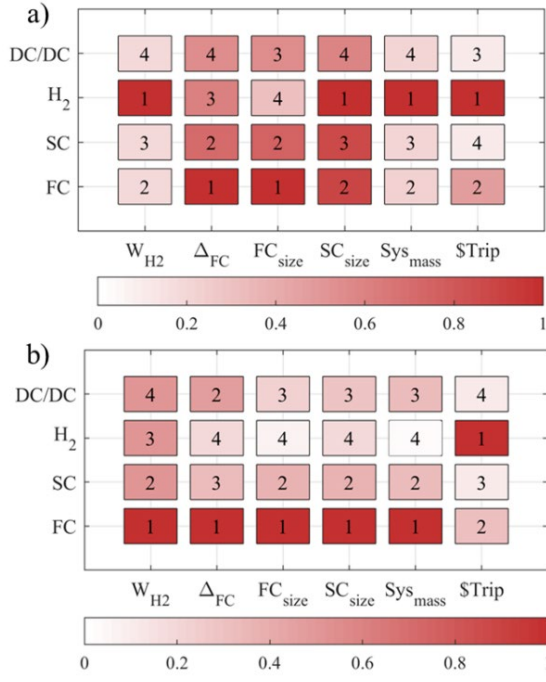


Fig. 6 Elementary effects of component price variation on system performance under (a) WMTC and (b) on-road driving cycle

B. Experimental test

Finally, the effect of component price variation is investigated using a HIL by comparing the performance of an EMS for three sets of weight and their corresponding optimal sizes obtained by the numerical simulation. The utilized EMS is based on online sequential quadratic programming (SQP) and the sizes are based on the reported values in Table IV. This test is deployed in a HIL setup, previously explained in Fig. 2. In this setup, the SC is a mathematical model, and the FC system is the real component. The FC output power in the HIL test bench is scaled up after the DC-DC converter to satisfy the demanded power. The EMS has been coded in LabVIEW environment and implemented in the real-time module of Compact-RIO by means of the block “Constrained Nonlinear Optimization virtual instrument VI”. Hereinafter, the implemented strategy is explained first. Subsequently, the obtained results are widely discussed.

1) Real-time instantaneous optimization

The energy management problem in a FCHEV is in principle a nonlinear optimization problem. It can be solved by SQP, which has gained optimal/sub-optimal results for a wide range of engineering problems, such as EMSs [42]. SQP is an iterative technique that solves nonlinear optimization problems by a QP subproblem at a given estimated solution. The application of SQP to the proposed multi-objective EMS at each step is considered in the following form:

$$\text{Min: } \$Trip_j = \$FC_{sys} \Delta_{FC,j} + \$H_2 W_{H_2,j} \quad j = 0, 1, 2 \dots \quad (31)$$

Subject to:

$$\begin{cases} 50 \% \leq SOC_{SC,j} \leq 90 \% \\ 0 A \leq i_{FC,j} \leq 42 A \\ -300 A \leq i_{SC,j} \leq 300 A \\ -0.1 P_{FC,max} \leq \Delta P_{FC,j} \leq 0.1 P_{FC,max} \end{cases} \quad (32)$$

The terms $\$SC \Delta_{trip,j}$ and $\$DC_{conv} \Delta_{trip,j}$, presented in the optimal optimization cost function in (22), are excluded for the online implementation. This is because they are the operational cost of SC and DC-DC converter and are calculated based on the driving profile time. If the vehicle is running, $\$SC \Delta_{trip,j}$ and $\$DC_{conv} \Delta_{trip,j}$ can be calculated and added to the total trip cost without participating in the optimization process. In the formulated problem, the optimization process is done for the defined MOCF (22).

2) Results

As presented in Table IV, the optimal sizes of components while using the MOCF with the highest price weights (FC_{sys} : 210 $\frac{\$}{kW}$, H_2 : 15 $\frac{\$}{kg}$, SC : 30 $\frac{\$}{Wh}$, DC_{con} : $\frac{150\$}{kW}$) are 21.2 kW for FC and 85.8 F for SC. In this section, these sizes are considered as the baseline. Then, using these baseline sizes, the online EMS based on SQP is employed to minimize the previously defined MOCF (31) for different cases:

- 1) “Highest price_{baseline size}”: It uses the highest reported prices of the components in Table II with the baseline size, as shown in Table IV (FC: 21.2 kW, SC: 85.8 F).
- 2) “FC cheap_{baseline size}”: It utilizes the highest prices for H_2 , SC , and DC_{con} , and the lowest price for FC_{sys} with the baseline sizes. This case study denotes an extreme price drop solely on the FC system.
- 3) “H2 cheap_{baseline size}”: It employs the highest prices for FC_{sys} , SC , and DC_{con} , and the lowest price for H_2 with the baseline sizes. In practice, this case study shows an extreme price drop down the hydrogen.
- 4) “FC cheap_{optimal size}”: It uses the same prices as FC cheap_{baseline size} but with the optimal sizes reported in Table IV (FC: 22.2 kW, SC: 63.5 F).
- 5) “H2 cheap_{optimal size}”: It utilizes the same prices as H2 cheap_{baseline size} but with the optimal sizes reported in Table IV (FC: 21.2 kW, SC: 94.8 F).

Fig. 7 shows a zoom on two time periods (from 1300 s to 1800 s and from 2300 s to 2800 s) of the drawn current from the FC system (i_{FC}) by the online EMS (Fig. 7a), the complete FC current profile (Fig. 7b), SOC variation of the SC (SOC_{SC}) (Fig. 7c), and the distribution of the i_{FC} (Fig. 7d) under Highest price_{baseline size}, FC cheap_{baseline size}, and H2 cheap_{baseline size} cases.

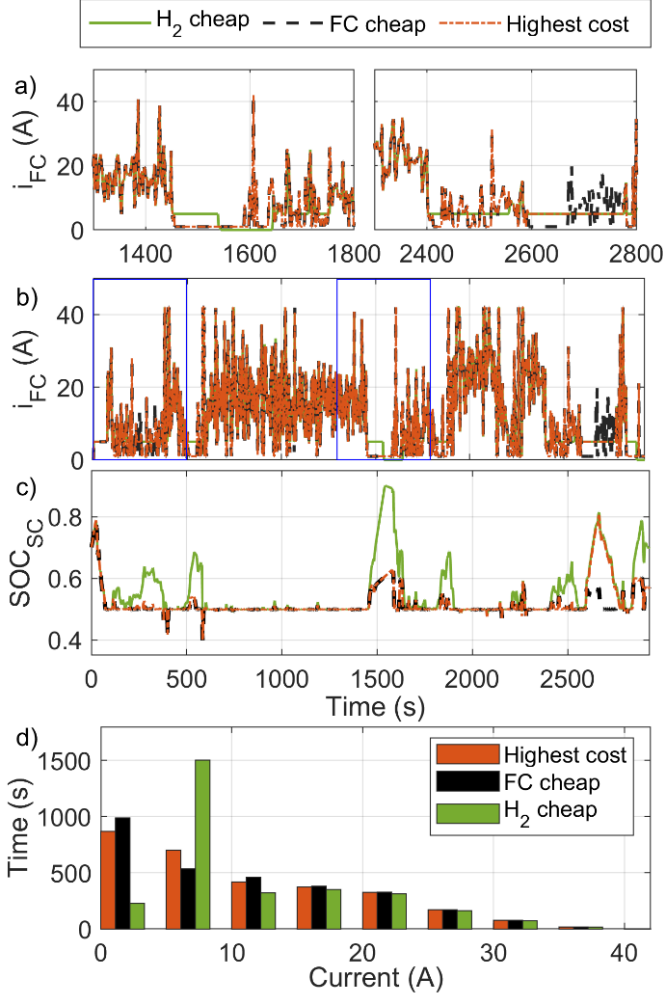


Fig. 7 HIL measurements during the on-road test, (a) a zoom on applied FC current from 1300 s to 1800 s range and 2300 s to 2800 s range, (b) the complete FC profile (c) SC SOC, (d) FC current distribution

As is seen in Fig. 7d, the H_2 cheap_{baseline size} case tends to avoid operating the FC in the low power region (k_1) most of the time. However, it has to turn off the FC at around 1544 s, as shown in Fig. 7a, since the SC has reached the maximum SOC level (90 %), as shown in Fig. 7c. FC cheap_{baseline size} case leads to the minimum power operation, as is seen after 2570 s in Fig. 7a. Contrary to the mentioned cases, the highest price case balances the FC degradation and hydrogen consumption by sustaining the SC charge around 50 % and switching to the low degradation region when the requested power is below the minimum, as observed in Fig. 7a around 2570 s. In this condition, SC absorbs this extra energy. The FC degradation distribution of each case is presented in Fig. 8. This representation corroborates that H_2 cheap_{baseline size} case minimizes the degradation due to low power operation at the cost of doubling the on/off cycle degradation (k_2).

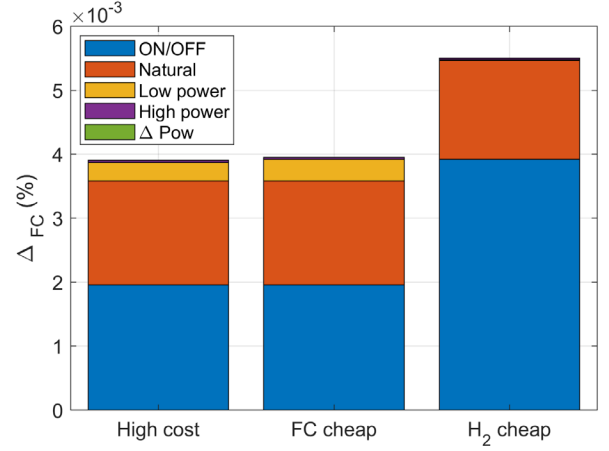


Fig. 8 FC degradation for each set of weights.

The system size, trip cost, total hydrogen consumption, and FC degradation of the five above-discussed cases are presented in Table V. The trip cost of each pair is comparable because they use the same component prices. From this table, the higher capacity of SC size in FC cheap_{optimal size} has led to less hydrogen consumption than FC cheap_{baseline size}. Moreover, H_2 cheap_{optimal size} has resulted in a lower trip compared to H_2 cheap_{baseline size} while having the same percentage of degradation. In fact, the lower system capacity in the latter has led to lower trip cost. It should be noted that the experimental case uses a H-500 low-power FC from Horizon which has a different polarization curve compared to the FCvelocity-9SSL from Ballard Power Systems. However, the optimized sizes obtained in previous section are still relevant. In the FC cheap case, the FC operates as a power following with a higher power FC, and in hydrogen cheap case, the FC operates with a more constant trend due to the higher SC low-pass filter effect.

TABLE V MULTI-OBJECTIVE COST FUNCTIONS COMPARISON

Cost function weights	Trips cost	H2 cons.	FC deg.
Highest price _{baseline size}	\$8.091	6.72 gr	0.0039 %
FC cheap _{baseline size}	\$7.065	6.73 gr	0.0040 %
H_2 cheap _{baseline size}	\$5.008	6.63 gr	0.0055 %
FC cheap _{optimal size}	\$6.668	6.65 gr	0.0040 %
H_2 cheap _{optimal size}	\$4.809	6.62 gr	0.0055 %

IV. CONCLUSIONS

This paper puts forward a SA to investigate the impact of price variation on the component sizing and energy management of a FCHEV. Since sizing and energy management problems have interdependencies, a two-step optimization method with a nested structure is utilized in this paper. The studied MOCF, composed of hydrogen cost, FC degradation cost, and operational costs of SC and DC-DC converter, is defined to optimize the trip cost. However, the performance of the MOCF relies on the defined weights that are based on the price range of the components. Therefore, this article puts forward a methodology for a SA to clarify the influence of the price range fluctuation over the sizing and total cost of the system. Therefore, this paper proposed a methodology to scrutinize the impact of component price

variation on the sizing and energy management of a FCHEV. The Morris or elementary effects (EE) method is used in this work due to its low computational within So, to analyze the results of this work, two phases of numerical simulation and experiments are considered. In the simulation phase, considering the use of the two-step optimization (GA for sizing and DP for power distribution) in the SA, it is realized that the FC and hydrogen prices are the dominant factors in sizing and the total price of the system. Hence, special attention needs to be paid to selecting those prices to avoid negative impacts on the sizing and EMS performance. It should be noted that the implemented methodology to study the SA and the two-step sizing optimization can be implemented in other engineering problems. In the experimental phase, the performance of an online EMS is investigated with the defined MOCF but with different price weights and sizes. To do so, a reduced-scale HIL set-up is used to deploy the strategy. The obtained results show that changing the price weights in a MOCF can result in more degradation and fuel consumption while using the same size. However, finding an optimal size for each price change on the MOCF can enhance the performance of the FCHEV up to 6 % in terms of the trip cost. This research demonstrates the impact of basic variation on FCHEV, which might help guide the automobile industry's future development and market strategy. Moreover, the presented sizing methodology could be implemented at early design phases to appropriately size the propulsion system of any electric vehicle as a function of actual or forecasted cost parameters. In future works, the developed SA methodology could be implemented to analyze the influence of external variables such as driving cycle average speed, maximum speed, ambient temperature, and FC temperature, on the fuel consumption and total trip cost. In addition, a more detailed study on the variation of the mass of the vehicle powertrain as well as different energy source combinations is required to provide an optimal power-source size map. Furthermore, future work could focus on increasing the FCHEV model accuracy in terms of hydrogen consumption and system degradation. Finally, the computing time could be reduced by implementing more recent optimization-based sizing methods.

VARIABLES

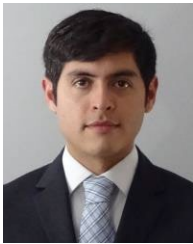
C_d	Typical aerodynamic drag coefficient
D^*	k -dimensional diagonal matrix
E_{Nernst}	Reversible voltage
E_i	Elementary effect of the i th parameter
F_{env}	Vehicle traction force resistance
F_{tr}	Traction force
G_{gb}	Gearbox transmission ratio
H_{FC}	Heat transfer coefficient
M_{O_2}	Oxygen molar mass
N_{FC}	Number of cells
$N_{SC,p}$	SC parallel branches
$N_{SC,s}$	SC connected in series
P^*	k -by- k random permutation matrix
$P_{FC,bus}$	Effective FC power in the DC bus
$P_{FC,max}$	FC maximum power
$P_{FC,sys}$	Fuel cell system power
P_{FC}	Fuel cell power
P_{SC}	Supercapacitor power
P_{comp}	Compressor power
P_{fan}	Fan electric power
P_{req}	Requested power
Q_{heat}	Residual energy
Q_{conv}	Heat dissipated due to convection
Q_{max}	SC maximum capacity
R_D	Equivalent diode resistance
R_{SC}	SC equivalent resistor
$R_{internal}$	Internal PEMFC resistor
SOC_{SC}	SC level of charge
T_{FC}	PEMFC stack temperature
T_{amb}	Ambient temperature
$T_{em,r}$	Reference torque
T_{em}	Electric machine torque
V_{EV}	Vehicle velocity
W_{H_2}	Consumed hydrogen flow
X^*	Base vector randomly selected
X_i	Independent input parameters
d_{ml}	Geometrical distance between all pairs of points
$i_{FC,max}$	Maximum FC current
i_{SC}	SC current
k_i	Semi-empirical FC degradation coefficient
t_i	Operational time
u_{DC}	DC bus voltage
u_{FC}	Cell voltage of a proton exchange membrane
u_{SC}	Supercapacitor voltage
u_{act}	Activation loss
u_c	Capacitance element OCV
u_{con}	Concentration loss
u_{ohmic}	Ohmic loss
ζ_n	Semi-empirical PEMFC resistor parameters
η_{FC}	System efficiency
η_{comp}	Compressor efficiency
η_{gb}	Gearbox transmission efficiency
η_m	Torque and drive efficiency
μ_{fr}	Typical rolling resistance coefficient
μ_i^*	Influence of the variable on the output
$\$DC_{conv}$	DC converter cost
$\$FC_{sys}$	FC system cost
$\$H_2$	Hydrogen cost
$\$SC$	SC cost
$\$Trip$	Trip cost
Δ_{FC}	FC degradation percentage
ΔP_{FC}	FC slew rate
Δ_{trip}	Normalized trip time
Ω_m	Rotor rotation speed
A_{aero}	Vehicle front area
B^*	Random trajectory
$C_{O_2}^*$	Oxygen concentration
$C_{SC,u}$	Single SC capacitance
C_{SC}	SC equivalent capacitance

ξ_n	Semi-empirical activation coefficients
ρ_{air}	Air density
B	Lower triangular matrix of ones
F	Faraday constant
g	Gravitational acceleration
m	Vehicle mass
r	Wheel radius
x	DP state variable
α	Semi-empirical diffusion mechanism parameter
β	Discrete braking mode value
γ	Specific heat ratio of the air
λ	Oxygen excess ratio constant

V. REFERENCES

- [1] F. Nadeem, S. M. S. Hussain, P. K. Tiwari, A. K. Goswami, and T. S. Ustun, "Comparative Review of Energy Storage Systems, Their Roles, and Impacts on Future Power Systems," *IEEE Access*, vol. 7, pp. 4555-4585, 2019.
- [2] M. A. Hannan, M. M. Hoque, A. Mohamed, and A. Ayob, "Review of energy storage systems for electric vehicle applications: Issues and challenges," *Renewable and Sustainable Energy Reviews*, vol. 69, pp. 771-789, 2017.
- [3] S. C. Konradt and H. Rottengruber, "Determination of the optimal battery capacity of a PEM fuel cell vehicle taking into account recuperation and supercapacitors," *Automotive and Engine Technology*, vol. 6, pp. 181-189, 2021/12/01 2021.
- [4] M. N. Boukoberine, T. Donato, and M. Benbouzid, "Optimized Energy Management Strategy for Hybrid Fuel Cell Powered Drones in Persistent Missions using Real Flight Test Data," *IEEE Transactions on Energy Conversion*, pp. 1-1, 2022.
- [5] Y. Zhou, A. Ravey, and M.-C. Péra, "Real-time cost-minimization power-allocating strategy via model predictive control for fuel cell hybrid electric vehicles," *Energy Conversion and Management*, vol. 229, p. 113721, 2021/02/01/ 2021.
- [6] Y. Liu, J. Li, Z. Chen, D. Qin, and Y. Zhang, "Research on a multi-objective hierarchical prediction energy management strategy for range extended fuel cell vehicles," *Journal of Power Sources*, vol. 429, pp. 55-66, 2019/07/31/ 2019.
- [7] X. Hu, J. Jiang, B. Egardt, and D. Cao, "Advanced Power-Source Integration in Hybrid Electric Vehicles: Multicriteria Optimization Approach," *IEEE Transactions on Industrial Electronics*, vol. 62, pp. 7847-7858, 2015.
- [8] T. Fletcher and K. Ebrahimi, "The Effect of Fuel Cell and Battery Size on Efficiency and Cell Lifetime for an L7e Fuel Cell Hybrid Vehicle," *Energies*, vol. 13, p. 5889, 2020.
- [9] G. Morrison, J. Stevens, and F. Joseck, "Relative economic competitiveness of light-duty battery electric and fuel cell electric vehicles," *Transportation Research Part C: Emerging Technologies*, vol. 87, pp. 183-196, 2018/02/01/ 2018.
- [10] A. Saltelli, K. Aleksankina, W. Becker, P. Fennell, F. Ferretti, N. Holst, et al., "Why so many published sensitivity analyses are false: A systematic review of sensitivity analysis practices," *Environmental Modelling & Software*, vol. 114, pp. 29-39, 2019/04/01/ 2019.
- [11] A. Saltelli, M. Ratto, T. Andres, F. Campolongo, J. Cariboni, D. Gatelli, et al., *Global sensitivity analysis: the primer*: John Wiley & Sons, 2008.
- [12] X. Wu, X. Hu, X. Yin, L. Li, Z. Zeng, and V. Pickert, "Convex programming energy management and components sizing of a plug-in fuel cell urban logistics vehicle," *Journal of Power Sources*, vol. 423, pp. 358-366, 2019/05/31/ 2019.
- [13] Y. Wang, S. J. Moura, S. G. Advani, and A. K. Prasad, "Power management system for a fuel cell/battery hybrid vehicle incorporating fuel cell and battery degradation," *International Journal of Hydrogen Energy*, vol. 44, pp. 8479-8492, 2019/03/29/ 2019.
- [14] P. G. Anselma and G. Belingardi, "Fuel cell electrified propulsion systems for long-haul heavy-duty trucks: present and future cost-oriented sizing," *Applied Energy*, vol. 321, p. 119354, 2022/09/01/ 2022.
- [15] A. M. Bassam, A. B. Phillips, S. R. Turnock, and P. A. Wilson, "Development of a multi-scheme energy management strategy for a hybrid fuel cell driven passenger ship," *International Journal of Hydrogen Energy*, vol. 42, pp. 623-635, 2017/01/05/ 2017.
- [16] J. M. Correa, F. A. Farret, V. A. Popov, and M. G. Simoes, "Sensitivity analysis of the modeling parameters used in Simulation of proton exchange membrane fuel cells," *IEEE Transactions on Energy Conversion*, vol. 20, pp. 211-218, 2005.
- [17] E. Borgonovo and E. Plischke, "Sensitivity analysis: A review of recent advances," *European Journal of Operational Research*, vol. 248, pp. 869-887, 2016/02/01/ 2016.
- [18] Y. Huang, H. Wang, A. Khajepour, B. Li, J. Ji, K. Zhao, et al., "A review of power management strategies and component sizing methods for hybrid vehicles," *Renewable and Sustainable Energy Reviews*, vol. 96, pp. 132-144, 2018/11/01/ 2018.
- [19] N. Leahey and J. Bauman, "A Fast Plant-Controller Optimization Process for Mild Hybrid Vehicles," *IEEE Transactions on Transportation Electrification*, vol. 5, pp. 444-455, 2019.
- [20] A. Macias, M. Kandidayeni, L. Boulon, and J. P. Trovão, "Fuel cell-supercapacitor topologies benchmark for a three-wheel electric vehicle powertrain," *Energy*, vol. 224, p. 120234, 2021/06/01/ 2021.
- [21] J. P. F. Trovão, M. Roux, M. Ê, and M. R. Dubois, "Energy- and Power-Split Management of Dual Energy Storage System for a Three-Wheel Electric Vehicle," *IEEE Transactions on Vehicular Technology*, vol. 66, pp. 5540-5550, 2017.
- [22] A. Bouscayrol, J.-P. Hautier, and B. Lemaire-Semail, "Graphic Formalisms for the Control of Multi-Physical Energetic Systems: COG and EMR," in *Systemic Design Methodologies for Electrical Energy Systems*, I. a. Wiley, Ed., ed, 2012, pp. 89-124.
- [23] G. Lopez Lopez, R. Schacht Rodriguez, V. M. Alvarado, J. F. Gomez-Aguilar, J. E. Mota, and C. Sandoval, "Hybrid PEMFC-supercapacitor system: Modeling and energy management in energetic macroscopic representation," *Applied Energy*, vol. 205, pp. 1478-1494, 2017.
- [24] J. P. Trovão, M. R. Dubois, M. Roux, E. Menard, and A. Desrochers, "Battery and Supercapacitor Hybridization for a Pure Electric Three-Wheel Roadster," in *2015 IEEE Vehicle Power and Propulsion Conference (VPPC)*, 2015, pp. 1-6.
- [25] R. F. Mann, J. C. Amphlett, M. A. I. Hooper, H. M. Jensen, B. A. Peppley, and P. R. Roberge, "Development and application of a generalised steady-state electrochemical model for a PEM fuel cell," *Journal of Power Sources*, vol. 86, pp. 173-180, 2000/03/01/ 2000.
- [26] M. Kandidayeni, H. Chaoui, L. Boulon, S. Kelouwani, and J. P. F. Trovão, "Online System Identification of a Fuel Cell Stack With Guaranteed Stability for Energy Management Applications," *IEEE Transactions on Energy Conversion*, vol. 36, pp. 2714-2723, 2021.
- [27] C. Wang, H. He, Y. Zhang, and H. Mu, "A comparative study on the applicability of ultracapacitor models for electric vehicles under different temperatures," *Applied Energy*, vol. 196, pp. 268-278, 2017/06/15/ 2017.
- [28] J. Wang, L. Zhang, J. Mao, J. Zhou, and D. Xu, "Fractional Order Equivalent Circuit Model and SOC Estimation of Supercapacitors for Use in HESS," *IEEE Access*, vol. 7, pp. 52565-52572, 2019.
- [29] A. Biswas and A. Emadi, "Energy Management Systems for Electrified Powertrains: State-of-the-Art Review and Future Trends," *IEEE Transactions on Vehicular Technology*, vol. 68, pp. 6453-6467, 2019.
- [30] K. Wang, N. Li, Y. Yang, S. Ke, Z. Zhang, M. Dou, et al., "Effect of load-cycling amplitude on performance degradation for proton exchange membrane fuel cell," *Chinese Chemical Letters*, 2021/02/23/ 2021.
- [31] S. Galla, A. Szweczyk, J. Smulko, and P. Przygocki, "Methods of Assessing Degradation of Supercapacitors by Using Various Measurement Techniques," *Applied Sciences*, vol. 9, 2019.
- [32] M. Kandidayeni, J. P. Trovão, M. Soleymani, and L. Boulon, "Towards health-aware energy management strategies in fuel cell hybrid electric vehicles: A review," *International Journal of Hydrogen Energy*, vol. 47, pp. 10021-10043, 2022/02/26/ 2022.
- [33] M. Yue, S. Jemei, R. Gouriveau, and N. Zerhouni, "Review on health-conscious energy management strategies for fuel cell hybrid electric vehicles: Degradation models and strategies," *International Journal of Hydrogen Energy*, vol. 44, pp. 6844-6861, 2019/02/18/ 2019.

- [34] T. Fletcher, R. Thring, and M. Watkinson, "An Energy Management Strategy to concurrently optimise fuel consumption & PEM fuel cell lifetime in a hybrid vehicle," *International Journal of Hydrogen Energy*, vol. 41, pp. 21503-21515, 2016.
- [35] H. Chen, P. Pei, and M. Song, "Lifetime prediction and the economic lifetime of Proton Exchange Membrane fuel cells," *Applied Energy*, vol. 142, pp. 154-163, 2015/03/15/ 2015.
- [36] K. Song, H. Chen, P. Wen, T. Zhang, B. Zhang, and T. Zhang, "A comprehensive evaluation framework to evaluate energy management strategies of fuel cell electric vehicles," *Electrochimica Acta*, vol. 292, pp. 960-973, 2018/12/01/ 2018.
- [37] U. S. D. o. Energy, "Fuel Cells," vol. Multi-Year Research, Development, and Demonstration Plan, 2017.
- [38] W. Zhou, L. Yang, Y. Cai, and T. Ying, "Dynamic programming for new energy vehicles based on their work modes Part II: Fuel cell electric vehicles," *Journal of Power Sources*, vol. 407, pp. 92-104, 2018/12/15/ 2018.
- [39] W. Zhou, L. Yang, Y. Cai, and T. Ying, "Dynamic programming for New Energy Vehicles based on their work modes part I: Electric Vehicles and Hybrid Electric Vehicles," *Journal of Power Sources*, vol. 406, pp. 151-166, 2018/12/01/ 2018.
- [40] K. Reddi, A. Elgowainy, N. Rustagi, and E. Gupta, "Impact of hydrogen refueling configurations and market parameters on the refueling cost of hydrogen," *International Journal of Hydrogen Energy*, vol. 42, pp. 21855-21865, 2017/08/24/ 2017.
- [41] E. G. Giakoumis, "Motorcycles," in *Driving and Engine Cycles*, E. G. Giakoumis, Ed., ed Cham: Springer International Publishing, 2017, pp. 167-191.
- [42] N. Andrei, "Sequential Quadratic Programming (SQP)," in *Continuous Nonlinear Optimization for Engineering Applications in GAMS Technology*, N. Andrei, Ed., ed Cham: Springer International Publishing, 2017, pp. 269-288.



Alvaro Macias F. (Member, IEEE) was born in Mexico City, in 1992. He received the B.S. degree in Mechatronics engineering from Tec de Monterrey, Guadalajara, Mexico, in 2015, the M.S. degree in electrical engineering in 2018 and the Ph.D. degree in electrical engineering in 2023, from *Université du Québec à Trois-Rivières* (UQTR), QC, Canada. He is currently a Post-Doctoral Researcher with the Moduly company in collaboration with the Hydrogen Research Institute, UQTR. He has been actively

involved in the research of energy management strategies for fuel cell systems, passive and active system configuration, energy storage systems and fuel cell modeling. His research interest includes energy-related topics, such as hybrid electric vehicles, fuel cell systems, energy management strategies, modeling, and control. Moreover, he has been a recipient of several awards/honors during his educational path, such as the Doctoral Scholarship from the *Fonds de recherche du Québec-Nature et technologies* (FRQNT), the scholarship for 3rd cycle from *Réseau Québécois sur l'Energie Intelligente* (RQEI) and the Post-Doctoral Scholarship from Mitacs with the Accelerate Entrepreneur program.



Mohsen Kandidayeni (Member, IEEE) was born in Tehran, Iran, in 1989. He received the B.S. degree in mechanical engineering in 2011, the master's degree (Hons.) in mechatronics from Arak University, Iran, in 2014, and the Ph.D. degree (Hons.) in electrical engineering from the University of Quebec at Trois-Rivières (UQTR), QC, Canada, in 2020. His educational journey has spanned through different paths. In 2016, he joined the Hydrogen Research Institute, UQTR. He is currently a Post-Doctoral

Researcher with the electric-Transport, Energy Storage and Conversion Lab (e-TESC), *Université de Sherbrooke*, and a Research Assistant with the Hydrogen Research Institute, UQTR. He has been actively involved in conducting research through authoring, coauthoring, and reviewing several articles in different prestigious scientific journals and also participating in various international conferences. His research interest includes energy-related topics, such as hybrid electric vehicles, fuel cell systems, energy management, multiphysics systems, modeling, and control. Moreover, he has been a recipient of several awards/honors during his educational path, such as the Doctoral

Scholarship from the *Fonds de recherche du Québec-Nature et technologies* (FRQNT), the Post-Doctoral Scholarship from FRQNT, the Excellence Student Grant from UQTR, and the Third Prize in Energy Research Challenge from the Quebec Ministry of Energy and Natural Resources.



Loïc Boulon (Senior Member, IEEE) received the master's degree in electrical and automatic control engineering from the University of Lille, France, in 2006, and the Ph.D. degree in electrical engineering from the University of Franche-Comté, France. Since 2010, he has been a Professor with UQTR, where he has been a Full Professor since 2016. Since 2019, he has been the Deputy Director of the Hydrogen Research Institute. His work deals with modeling, control, and energy management of multiphysics systems. He has published more than 120 scientific

articles in peer-reviewed international journals and international conferences, and given over 35 invited conferences all over the world. His research interests include hybrid electric vehicles and energy and power sources, such as fuel cell systems, batteries, and ultracapacitors. In 2015, he was the General Chair of the IEEE-Vehicular Power and Propulsion Conference in Montréal, QC, Canada. He is also the VP of Motor Vehicles of the IEEE Vehicular Technology Society and the Founder of the International Summer School on Energetic Efficiency of Connected Vehicles and the IEEE VTS Motor Vehicle Challenge. He is also the holder of the Canada research chair position of energy sources for the vehicles of the future



João Pedro F. Trovão (Senior Member, IEEE) received the M.Sc. and Ph.D. degrees in electrical engineering from the University of Coimbra, Coimbra, Portugal, in 2004 and 2013, respectively. From 2000 to 2014, he was a Teaching Assistant and an Assistant Professor with the Polytechnic Institute of Coimbra—Coimbra Institute of Engineering (IPC—ISEC), Portugal. Since 2014, he has been a Professor with the Department of Electrical Engineering and Computer Engineering, University

of Sherbrooke, Sherbrooke, QC, Canada, where he currently holds the Canadian research chair position in efficient electric vehicles with the Hybridized Energy Storage Systems. He is also the Founding Member and the Director of the electric-Transport, Energy Storage and Conversion (e-TESC) Lab, University of Sherbrooke. He is the author/coauthor of over 175 journal articles and conference papers. His research interests cover the areas of electric vehicles, hybridized energy storage systems, energy management, and rotating electrical machines. He was the General Chair of the 2018 IEEE Vehicle Power and Propulsion Conference, Chicago, IL, USA. He was a Guest Editor for the Special Issue of *IET Electrical Systems in Transportation* on energy storage and electric power sub-systems for advanced vehicles and the Special Issue of IEEE TRANSACTIONS ON VEHICULAR TECHNOLOGY on electric powertrains for future vehicles and on advanced vehicle power propulsion systems. He is also a Senior Editor of the automotive electronics topic of the *IEEE Vehicular Technology Magazine*.